

# An Interconnect Energy Model Considering Coupling Effects

Taku Uchino and Jason Cong, *Fellow, IEEE*

**Abstract**—This paper presents an analytical interconnect energy model with consideration of coupling effects, including crosstalk and glitch, which are not adequately considered by the conventional  $(1/2)CV^2$  model. The energy model introduces a new time-scale parameter, called the *charge time*, which represents the correlation time length between two events and is considered to be the counterpart of the Elmore delay. The authors' energy model is more accurate than the  $(1/2)CV^2$  model with the same time complexity. Experimental results show that their algorithm is several orders of magnitude faster than HSPICE with less than 5% error. In comparison, the error of the  $(1/2)CV^2$  model can be as high as 100%. The authors further investigate the relationship between interconnect energy and signal correlation and propose a simplified model, which is even faster than their basic model. This paper also discusses ongoing issues of their model, including stability analysis, event propagation, and resistive shielding effects in interconnect energy calculation.

**Index Terms**—Coupling effects, interconnect energy model, power estimation.

## I. INTRODUCTION

IN THE deep submicron design of integrated circuits, the analog behavior of interconnects becomes critical in determining system performance, reliability, and power. This requires early interconnect estimation, which has been difficult in the conventional logic-centric design flow. To overcome this difficulty, an interconnect-centric design flow has been proposed [1], in which the interconnect topology and geometry is determined at early design stages. This makes it possible to estimate interconnect delay, noise, and power at the early design stages, provided we have accurate interconnect models.

For interconnect power modeling, the  $(1/2)CV^2$  model has been commonly used. This model is based on the assumption that each event (i.e., rise or fall transition) consumes energy  $(1/2)CV_{DD}^2$ , where  $C$  is the load capacitance and  $V_{DD}$  is the supply voltage. Although this model is simple and easy to deal with, it is not accurate in the deep submicron design. Fig. 1 shows that the error of the  $(1/2)CV^2$  model becomes large for long interconnects under the 70-nm technology derived from NTRS'97 [1], [2]. The error is due to the following coupling effects.

Manuscript received October 9, 2001. This work was supported in part by the National Science Foundation under Award CCR-0096383. This paper was presented in part at the 36th Design Automation Conference, New Orleans, LA, 1999. This paper was recommended by Associate Editor M. Sarrafzadeh.

T. Uchino is with the STI-Design Center, Toshiba America Electronic Components, Austin, TX 78758 USA (e-mail: taku.uchino@toshiba.co.jp).

J. Cong is with the Computer Science Department, University of California, Los Angeles, CA 90095 USA (e-mail: cong@cs.ucla.edu).

Publisher Item Identifier S 0278-0070(02)05624-5.

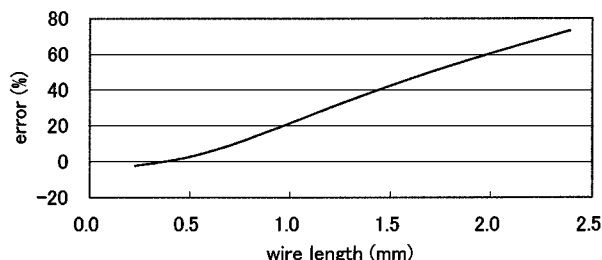


Fig. 1. Error of  $(1/2)CV^2$  model compared with HSPICE. The circuit is composed of ten parallel equal-length interconnects with minimum width and spacing under the 70-nm technology. The load capacitance (“ $C$ ”) for each interconnect is the sum of the ground and coupling capacitances. The horizontal axis represents the length of these interconnects. The input waveform is randomly generated in such a way that the time interval between successive events is 40–1000 ps.

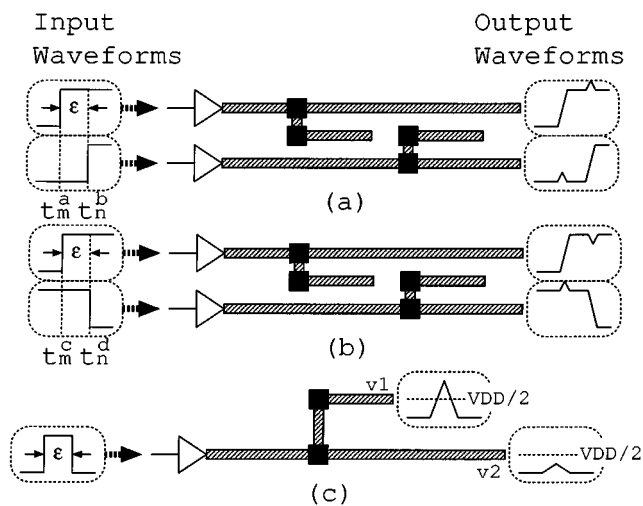


Fig. 2. Coupling effects. The waveforms on the left represent the input waveforms, where  $\epsilon$  represents the time difference between the events. The waveforms at the far ends of the interconnects are shown on the right. (a) and (b) illustrate the mutual coupling, and (c) illustrates the self coupling.

**Mutual Coupling (Crosstalk):** Events on different interconnects can interfere with each other through the coupling capacitance. Fig. 2(a) and (b) illustrate the mutual coupling.

**Self Coupling (Glitch or Noise):** Successive events on one interconnect can interfere with each other in the sense that the first event may not completely charge/discharge the interconnect before the second event begins to discharge/charge the same interconnect. Fig. 2(c) illustrates the self-coupling.

To see the importance of the coupling effects in energy estimation, we investigate simple interconnect models shown in

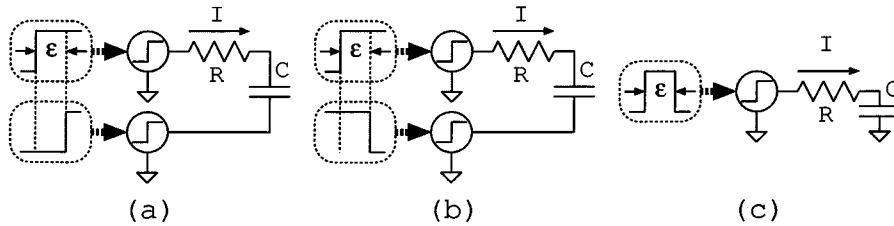


Fig. 3. Simple examples to illustrate coupling effects.

Fig. 3, where  $I$ ,  $R$ , and  $C$  represent the current, resistance, and coupling capacitance [Fig. 3(a) and (b)] or ground capacitance [Fig. 3(c)], respectively. The ground capacitance is ignored in Fig. 3(a) and (b).

According to the  $(1/2)CV^2$  model, the interconnect energy is  $2 \times (1/2)CV_{DD}^2 = CV_{DD}^2$  for each case in Fig. 3. On the other hand, careful analysis gives the following energy:

$$E = CV_{DD}^2 \left( 1 \pm \exp\left(-\frac{\epsilon}{RC}\right) \right) \quad (1)$$

where “-” sign is for Fig. 3(a) and (c), and “+” sign is for Fig. 3(b). Equation (1) is obtained by inserting the solution of the circuit equations into the interconnect energy defined by  $E \equiv \int dt RI^2$ , where  $t$  is the time, and  $RI^2$  is the power. The coupling effects are represented by the term  $\exp(-\epsilon/RC)$  in (1), which can range from 0 to 1. This means that the interconnect energy heavily depends on the coupling effects.

To incorporate the mutual coupling effects into the  $(1/2)CV^2$  model, Kim *et al.* [3] proposed a power model considering the time difference between two transitions. They implicitly assumed that their model parameter  $\beta$  is independent of the interconnect topology and geometry.

The self-coupling effects were considered in several papers [4]–[6]. However, the interconnect topology and geometry was not adequately considered since they were focused on the glitch power of the logic gates.

This paper proposes an analytical interconnect energy model unifying the mutual and self-coupling effects, which were dealt with differently in the previous works. Since our model is based on the interconnect topology and geometry, it is useful in the interconnect-centric design flow. Our model introduces a new time-scale parameter, called the *charge time*, which represents the correlation time length between two events. The charge time is considered to be the power counterpart of the Elmore delay due to their similarities.

The paper is organized as follows: Section II is devoted to the definitions and assumptions of the interconnect model used in this paper. Section III derives our interconnect energy model. Section IV explains our model with examples. Section V proposes an algorithm to calculate the charge time. Section VI presents an event-driven energy calculation algorithm. Section VII discusses the relation between energy and signal correlation. Section VIII shows the total flow of our interconnect energy calculation. Section IX shows the experimental results. Section X introduces a few important features of our model to be investigated in the future works, and Section XI concludes the paper.

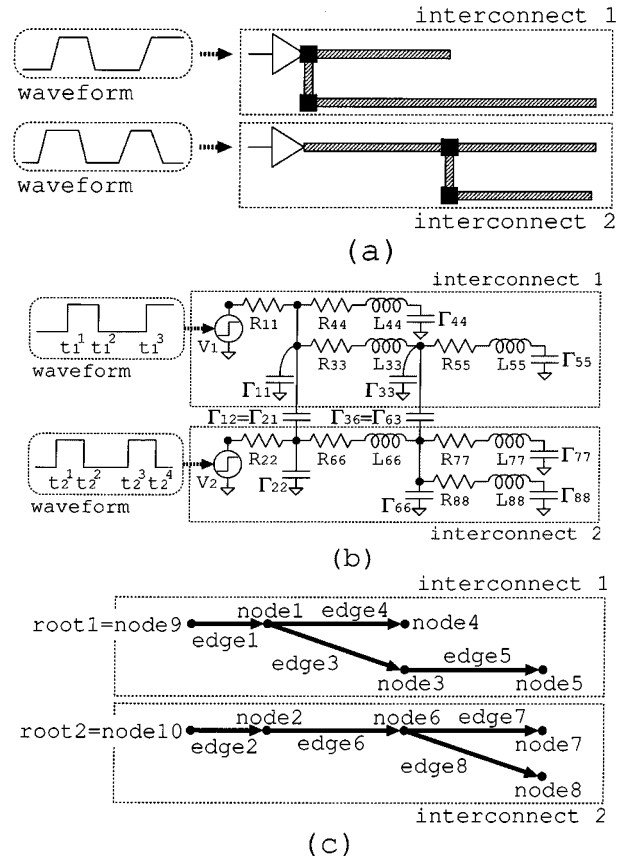


Fig. 4. Interconnect modeling. (a) Physical implementation of interconnects. (b) RCL model after driver modeling. (c) Graphical representation of (b).

## II. INTERCONNECT MODELING

### A. Overview of Our Interconnect Modeling

We assume that repeaters have been adequately inserted for long interconnects, and an interconnect in this paper represents the set of the wire segments in one stage driven by a repeater or driver as shown in Fig. 4(a). For simplicity, a repeater is also called a driver.

Each wire segment is modeled by a lumped RCL element, and the mutual inductances and coupling capacitances are considered as the interaction among these elements as shown in Fig. 4(b). These elements compose an *interconnect graph* shown in Fig. 4(c).

Each driver is modeled by a voltage source and an output resistance as will be explained in Section II-D. An output resistance is represented by an edge in the interconnect graph. For example, edges 1 and 2 in Fig. 4(c) represent the output resistances  $R_{11}$  and  $R_{22}$  in Fig. 4(b), respectively.

Sections II-B–E go into details of our interconnect modeling.

### B. Graph Structure

The nodes and edges in the interconnect graph are defined as follows:

- (G1) Each node represents either the voltage source of a driver, a sink<sup>1</sup>, or a joint of wire segments.
- (G2) Each edge represents either the output resistance of a driver or a wire segment.

The node representing the voltage source of a driver is called the *root*. The root is always connected to only one edge representing the output resistance of the driver.

An interconnect is a directed tree. The direction of an edge is consistent with the path from the root to a sink. In other words, any edge points to the downstream.

Let  $M$  and  $N$  denote the number of the interconnects and the number of the edges, respectively. Since each interconnect is a tree, the total number of nodes in our model is  $M + N$ . The labels for nodes and edges are defined in such a way that we have the following.

- (L1) Edge  $m$  ( $m = 1, \dots, M$ ) represents the output resistance of the driver in interconnect  $m$ .
- (L2) Node  $N + m$  ( $m = 1, \dots, M$ ) is the root of interconnect  $m$ , called the root  $m$ .

The labels for the other edges and nodes can be determined arbitrarily. These labeling rules are illustrated in Fig. 4(c), where  $M = 2$  and  $N = 8$ .

### C. Electrical Properties

Let  $V_m(t)$  denote the voltage of root  $m$  at time  $t$ . Since each transition of  $V_m$  is modeled by a step function (as will be described in Section II-D), the time derivative of  $V_m(t)$  is expressed as

$$\dot{V}_m(t) = \sum_{a=1}^{w_m} \delta(t - t_m^a) \Delta V_m^a \quad (2)$$

where  $w_m$  is the number of the events on root  $m$ ,  $\delta(t)$  is the  $\delta$ -function,  $t_m^a$  ( $a = 1, 2, \dots, w_m$ ) is the time of event  $a$ , and  $\Delta V_m^a$  is the change of  $V_m(t)$  at  $t_m^a$ . Note that  $\Delta V_m^a = \pm V_{DD}$  in digital circuits since  $V_m(t)$  is either 0 or  $V_{DD}$ . We assume  $t_m^a > 0$ , and  $t_m^a < t_m^b$  if and only if  $a < b$ .

The *resistance matrix*  $R$  is an  $N \times N$  diagonal matrix, where  $R_{ii}$  is the resistance of edge  $i$ .

The *inductance matrix*  $L$  is an  $N \times N$  symmetric matrix, where  $L_{ij}$  ( $i \neq j$ ) is the mutual inductance between edges  $i$  and  $j$ , and  $L_{ii}$  is the self-inductance of edge  $i$ .

The *capacitance matrix*  $C$  is an  $N \times N$  symmetric matrix, whose elements are defined by

$$C_{vv} \equiv \sum_{w=1}^N \Gamma_{vw}, \quad C_{vw} \equiv -\Gamma_{vw} \quad (v \neq w) \quad (3)$$

where  $\Gamma_{vv}$  is the ground capacitance<sup>2</sup> of node  $v$ , and  $\Gamma_{vw}$  ( $v \neq w$ ) is the coupling capacitance between nodes  $v$  and  $w$ .

<sup>1</sup>A sink is a terminal pin which receives a signal from the driver.

<sup>2</sup>The ground capacitance includes the area and fringe wire capacitance and the sink capacitance, if any.

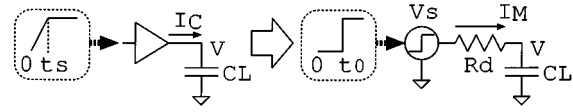


Fig. 5. Driver modeling. The CMOS driver with the input waveform on the left is modeled by the output resistance with the voltage source on the right.

### D. Driver Modeling

For simplicity, we assume the driver is a one-input and one-output buffer as shown in the left-hand side of Fig. 5, where  $C_L$  is the load capacitance and  $t_s$  is the transition time of the input signal. This driver is modeled by an output resistance  $R_d$  and a voltage source  $V_S$  switching instantly at time  $t_0$  as shown in the right-hand side of Fig. 5. To determine the model parameters  $R_d$  and  $t_0$ , we compare the output current of the CMOS driver ( $I_C$ ) with that of the model ( $I_M$ ) using the moment matching method.

Note that the Laplace transform of  $I_M$  is expressed as

$$\int_0^{\infty} dt e^{-st} I_M(t) = \frac{C_L \Delta V}{1 + s R_d C_L} e^{-st_0} \quad (4)$$

where  $\Delta V \equiv V(\infty) - V(0)$  is the change of the voltage. Replacing  $I_M$  with  $I_C$  in (4), we obtain the following equation:

$$\int_0^{\infty} dt e^{-st} I_C(t) \approx \frac{C_L \Delta V}{1 + s R_d C_L} e^{-st_0}. \quad (5)$$

Expanding both sides of (5) around  $s = 0$ , and comparing the coefficients of  $s^n$  ( $n = 1, 2$ ), we obtain

$$R_d^2 C_L^2 = a_2 - a_1^2, \quad t_0 + R_d C_L = a_1 \quad (6)$$

where

$$a_n \equiv \frac{1}{C_L \Delta V} \int_0^{\infty} dt t^n I_C(t) \quad (n = 1, 2)$$

are moments of  $I_C$ , which can be measured by HSPICE. Solving (6), we obtain  $R_d$  and  $t_0$ . Since  $R_d$  and  $t_0$  are functions of  $C_L$ ,  $t_s$ , and the switching condition (rise/fall), we can make lookup tables for  $R_d$  and  $t_0$  with these variables.

### E. Driver Internal Energy

The driver internal energy per event  $E_{\text{int}}$  is modeled by

$$E_{\text{int}} = E_{\text{total}} - \frac{1}{2} C_L \Delta V^2 \quad (7)$$

where  $E_{\text{total}}$  is the total energy including interconnect energy as well as driver internal energy.  $E_{\text{total}}$  can be measured by HSPICE. Since  $E_{\text{int}}$  is a function of  $C_L$ ,  $t_s$ , and the switching condition, we can also make a lookup table for  $E_{\text{int}}$  with these variables.

## III. DERIVATION OF OUR ENERGY MODEL

This section derives our energy model using the Kirchhoff's Current law (KCL) and Kirchhoff's Voltage law (KVL) equations for the modeled RCL circuit.

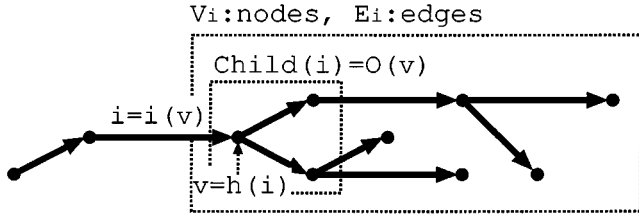


Fig. 6. Example of  $i(v)$ ,  $O(v)$ ,  $h(i)$ ,  $\mathcal{V}_i$ ,  $\mathcal{E}_i$ , and  $\text{Child}(i)$ .

### A. Incidence Matrix

This subsection provides useful properties of the incidence matrix for the interconnect graph.

The *incidence matrix*  $A$  is an  $(M+N) \times N$  matrix such that  $A_{vi} = 1$  ( $A_{vi} = -1$ ) if node  $v$  is the head (tail)<sup>3</sup> of edge  $i$ , and  $A_{vi} = 0$  otherwise. Note that the incidence matrix  $A$  satisfies

$$\sum_{i=1}^N A_{vi} x_i = x_{i(v)} - \sum_{i \in O(v)} x_i \quad (8)$$

for any  $x_1, x_2, \dots, x_N$ , where  $i(v)$  is the edge incoming to node  $v$ , and  $O(v)$  is the set of the edges outgoing from node  $v$  (cf. Fig. 6).

Using labeling rules (L1) and (L2),  $A$  is expressed as

$$A = \begin{bmatrix} A_r \\ -\vec{c}_1^T \\ -\vec{c}_2^T \\ \vdots \\ -\vec{c}_M^T \end{bmatrix}, \quad \vec{c}_m \equiv \begin{bmatrix} 0 \\ \vdots \\ 0 \\ 1 \\ 0 \\ \vdots \\ 0 \end{bmatrix} \leftarrow m\text{th row} \quad (9)$$

where the row vector  $\vec{c}_m^T$  ( $m = 1, 2, \dots, M$ ) is the transpose<sup>4</sup> of the column vector  $\vec{c}_m$ . The  $N \times N$  matrix  $A_r$  in (9) is called the *reduced incidence matrix*.  $A_r$  is invertible since the interconnect graph is a set of trees. The inverse  $A_r^{-1}$  satisfies the property that

$$(A_r^{-1})_{iv} = \begin{cases} 1, & (v \in \mathcal{V}_i) \\ 0, & (v \notin \mathcal{V}_i) \end{cases} \quad (10)$$

where  $\mathcal{V}_i$  is the set of the nodes in the subtree rooted at the head of edge  $i$  (cf. Fig. 6). The proof of (10) is as follows.

*Proof:* Let  $B$  denote the matrix whose components are defined by the right-hand side of (10), i.e.,  $B_{iv} = 1$  ( $= 0$ ) if  $v \in \mathcal{V}_i$  ( $v \notin \mathcal{V}_i$ ). We will prove  $BA_r \vec{x} = \vec{x}$  for any vector  $\vec{x}$ , since it implies  $B = A_r^{-1}$ . Using (8), we obtain

$$(BA_r \vec{x})_i = \sum_{w \in \mathcal{V}_i} x_{i(w)} - \sum_{v \in \mathcal{V}_i} \sum_{j \in O(v)} x_j. \quad (11)$$

Note that each  $j \in O(v)$  is the incoming edge of some node  $w$  in  $\mathcal{V}_i$ . In other words, there exists  $w \in \mathcal{V}_i$  such that  $j = i(w)$ . This means each  $x_j$  in the second term of (11) is canceled out by the first term  $x_{i(w)}$  for some node  $w \in \mathcal{V}_i$ , and we are left with  $x_i$  since there is no node  $v \in \mathcal{V}_i$  such that  $i \in O(v)$ . Hence  $(BA_r \vec{x})_i = x_i$ . ■

<sup>3</sup>The *head* (*tail*) of an edge is the node to (from) which the edge is incoming (outgoing).

<sup>4</sup>The transpose of matrix  $X$  is denoted by  $X^T$ .

### B. KCL and KVL Equations

Using  $\Gamma_{vw}$  or  $C$  (capacitance matrix) defined in Section II-C, the charge of node  $v$ , i.e.,  $q_v$ , is expressed as

$$q_v = \Gamma_{vv} U_v + \sum_{w \neq v} \Gamma_{vw} (U_v - U_w) = \sum_{w=1}^N C_{vw} U_w \quad (12)$$

where  $U_v$  ( $U_w$ ) is the voltage of node  $v$  ( $w$ ). On the other hand, the current conservation implies

$$\dot{q}_v = I_{i(v)} - \sum_{i \in O(v)} I_i = \sum_{i=1}^N (A_r)_{vi} I_i \quad (13)$$

where  $\dot{q}_v$  is the time derivative of  $q_v$ ,  $I_i$  is the current of edge  $i$ , and we used (8). From (12) and (13), we obtain

$$C \dot{\vec{U}} = A_r \vec{I} \quad (14)$$

where  $\vec{U}$  ( $\vec{I}$ ) denotes the voltage (current) vector whose  $v$ th ( $i$ th) element is  $U_v$  ( $I_i$ ). Equation (14) represents the KCL equation for the coupled interconnects.

Considering the voltage drop for each edge, the KVL equation is obtained as follows:

$$R \vec{I} + L \dot{\vec{I}} = \sum_{m=1}^M \vec{c}_m V_m - A_r^T \vec{U}. \quad (15)$$

Equations (14) and (15) can be also expressed as

$$\check{C} \dot{\vec{U}} = \vec{I}, \quad R \vec{I} + L \dot{\vec{I}} = \sum_{m=1}^M \vec{c}_m V_m - \vec{U} \quad (16)$$

where  $\vec{U} \equiv A_r^T \vec{U}$ , and  $\check{C} \equiv A_r^{-1} C A_r^{-1T}$ . Using (10), the  $(i, j)$  element of  $\check{C}$  is expressed as

$$\check{C}_{ij} = \sum_{v \in \mathcal{V}_i} \sum_{w \in \mathcal{V}_j} C_{vw}. \quad (17)$$

Especially when  $i = m$  and  $j = n$  where  $m, n = 1, \dots, M$ , (17) becomes as follows:

$$\check{C}_{mm} = \sum_{n=1}^M \tilde{\Gamma}_{mn}, \quad \check{C}_{mn} = -\tilde{\Gamma}_{mn} \quad (m \neq n) \quad (18)$$

where  $\tilde{\Gamma}_{mm} \equiv \sum_{v \in \mathcal{V}_m} \Gamma_{vv}$  is the total ground capacitance of interconnect  $m$ , and  $\tilde{\Gamma}_{mn} \equiv \sum_{v \in \mathcal{V}_m} \sum_{w \in \mathcal{V}_n} \Gamma_{vw}$  ( $m \neq n$ ) is the total coupling capacitance between interconnects  $m$  and  $n$ . Hence,  $\check{C}_{mm}$  is the total load capacitance of interconnect  $m$ .

### C. Solution for KCL and KVL Equations

Equation (16) can be combined into the following single matrix equation:

$$\dot{\vec{x}} = Q(\vec{x} - \vec{b}) \quad (19)$$

where

$$\vec{x} \equiv \begin{bmatrix} \vec{U} \\ \vec{I} \end{bmatrix}, \quad \vec{b} \equiv \sum_{m=1}^M \begin{bmatrix} \vec{c}_m \\ 0 \end{bmatrix} V_m \quad (20)$$

and

$$Q \equiv \begin{bmatrix} \tilde{C}^{-1} & 0 \\ 0 & -L^{-1} \end{bmatrix} \begin{bmatrix} 0 & 1 \\ 1 & R \end{bmatrix}.$$

Using the method of constant variation, the solution of (19) is expressed as

$$\vec{x}(t) = \vec{b}(t) - \int_0^t d\xi e^{Q(t-\xi)} \dot{\vec{b}}(\xi) \quad (21)$$

with initial condition  $\vec{x}(0) = \vec{b}(0)$ , i.e.,  $I_i(0) = 0$  and  $U_v(0) = V_m(0)$  for  $v \in \mathcal{V}_m$ , which means the circuit is static at time  $t = 0$ .

#### D. Energy Dissipation

The total interconnect energy  $E$  is defined by the integral of the power as follows:

$$E \equiv \int_0^\infty dt \sum_{j=1}^N R_{jj} I_j^2 = \int_0^\infty dt \vec{I}^T R \vec{I}. \quad (22)$$

Using  $\vec{x}$  defined in (20) and (22) we have

$$E = \int_0^\infty dt \vec{x}^T \begin{bmatrix} 0 & 0 \\ 0 & R \end{bmatrix} \vec{x}. \quad (23)$$

Inserting (21) into (23), we obtain

$$E = \int_0^\infty dt \int_0^t d\xi \int_0^t d\xi' \dot{\vec{b}}^T(\xi) F(t; \xi, \xi') \dot{\vec{b}}(\xi') \quad (24)$$

where matrix  $F(t; \xi, \xi')$  is defined by

$$F(t; \xi, \xi') \equiv e^{Q^T(t-\xi)} \begin{bmatrix} 0 & 0 \\ 0 & R \end{bmatrix} e^{Q(t-\xi')}.$$

Note that  $F(t; \xi, \xi')$  is a total derivative, i.e.,

$$F(t; \xi, \xi') = \frac{d}{dt} G(t; \xi, \xi') \quad (25)$$

where

$$G(t; \xi, \xi') \equiv -\frac{1}{2} e^{Q^T(t-\xi)} \begin{bmatrix} \tilde{C} & 0 \\ 0 & L \end{bmatrix} e^{Q(t-\xi')}.$$

Inserting (25) into (24), and changing the order of the integration, we obtain

$$E = \int_0^\infty d\xi \int_0^\infty d\xi' \int_{\max(\xi, \xi')}^\infty dt \frac{d}{dt} \times \left( \dot{\vec{b}}^T(\xi) G(t; \xi, \xi') \dot{\vec{b}}(\xi') \right).$$

Carrying out the integration over  $t$ , we obtain

$$E = \sum_{m=1}^M \sum_{n=1}^M E_{mn} \quad (26)$$

where

$$E_{mn} \equiv \frac{1}{2} \int_0^\infty d\xi \int_0^\infty d\xi' H_{mn}(|\xi - \xi'|) \dot{V}_m(\xi) \dot{V}_n(\xi') \quad (27)$$

and

$$H_{mn}(t) \equiv [\tilde{e}_m^T \tilde{C} \quad 0] e^{Qt} \begin{bmatrix} \tilde{e}_n \\ 0 \end{bmatrix}. \quad (28)$$

Note that  $H_{mn}(t)$  is symmetric with respect to  $m$  and  $n$

$$H_{mn}(t) = H_{nm}(t). \quad (29)$$

In the above derivation, we used the stability condition

$$\lim_{t \rightarrow \infty} e^{Qt} = 0 \quad (30)$$

which means any eigenvalue of  $Q$  has the negative real part. This can be proved using the fact that matrices  $R$ ,  $C$ , and  $L$  are real, symmetric, and positive definite. The complete proof can be found in [8]. Equation (30) also implies

$$\lim_{t \rightarrow \infty} H_{mn}(t) = 0. \quad (31)$$

#### E. Model Order Reduction

Since  $H_{mn}(t)$  contains a large matrix  $Q$ , we apply the moment matching method [9] to  $H_{mn}(t)$ .

Inserting (28) into the Laplace transform of  $H_{mn}(t)$  defined by

$$\tilde{H}_{mn}(s) \equiv \int_0^\infty dt e^{-st} H_{mn}(t)$$

we obtain

$$\tilde{H}_{mn}(s) = [\tilde{e}_m^T \tilde{C} \quad 0] (s - Q)^{-1} \begin{bmatrix} \tilde{e}_n \\ 0 \end{bmatrix}. \quad (32)$$

Expanding (32) around  $s = 0$ , we obtain

$$\tilde{H}_{mn}(s) = M_{mn}^{(0)} - sM_{mn}^{(1)} + s^2M_{mn}^{(2)} - \dots$$

where

$$M_{mn}^{(0)} = (\tilde{C}R\tilde{C})_{mn} \quad (33)$$

$$M_{mn}^{(1)} = \left( \tilde{C}(R\tilde{C}R - L)\tilde{C} \right)_{mn} \quad (34)$$

$$M_{mn}^{(2)} = \left( \tilde{C}(R\tilde{C}R\tilde{C}R - R\tilde{C}L - L\tilde{C}R)\tilde{C} \right)_{mn} \quad (35)$$

are moments of  $H_{mn}(t)$ . We also define moment  $M_{mn}^{(-1)}$  as

$$M_{mn}^{(-1)} \equiv H_{mn}(t=0) = \tilde{C}_{mn}. \quad (36)$$

Using these moments, the one- and two-pole models for  $H_{mn}(t)$  are obtained as follows.

1) *One-Pole Model:* In the one-pole model,  $H_{mn}(t)$  is approximated by  $f(t) \equiv r e^{pt}$ . The parameters  $r$  and  $p$  are determined by the conditions  $H_{mn}(t=0) = f(t=0)$  and  $\tilde{H}_{mn}(s=0) = \tilde{f}(s=0)$ , where  $\tilde{f}(s)$  is the Laplace transform of  $f(t)$ . The result is as follows:

$$H_{mn}(t) \approx M_{mn}^{(-1)} e^{-tM_{mn}^{(-1)}/M_{mn}^{(0)}}. \quad (37)$$

Note that inductance does not appear in this model.

2) *Two-Pole Model:* The two-pole model is shown only for reference.

In the two-pole model,  $H_{mn}(t)$  is approximated by  $f(t) \equiv r_1 e^{p_1 t} + r_2 e^{p_2 t}$ . The parameters  $r_1, r_2, p_1$ , and  $p_2$  are determined by the conditions  $H_{mn}(t=0) = f(t=0)$ ,  $\tilde{H}_{mn}^{(n)}(s=0) = \tilde{f}^{(n)}(s=0)$  ( $n = 0, 1, 2$ ), where  $\tilde{f}(s)$  is the Laplace transform of  $f(t)$ , and  $\tilde{H}_{mn}^{(n)}$  ( $\tilde{f}^{(n)}$ ) is the  $n$ th derivative with respect to  $s$ . The result is as follows:

$$H_{mn}(t) \approx \begin{cases} e^{-\alpha t} (q \cosh \beta t + r \sinh \beta t) & (D > 0) \\ e^{-\alpha t} (q + r \beta t) & (D = 0) \\ e^{-\alpha t} (q \cos \beta t + r \sin \beta t) & (D < 0) \end{cases}$$

where

$$D \equiv B_1^2 - 4B_0B_2, \quad \alpha \equiv \frac{B_1}{2B_2}, \quad \beta \equiv \frac{\sqrt{|D|}}{2B_2}$$

$$q \equiv M_{mn}^{(-1)}, \quad r \equiv \frac{(2M_{mn}^{(0)}B_0 - M_{mn}^{(-1)}B_1)}{\sqrt{|D|}}$$

$$B_0 \equiv M_{mn}^{(-1)}M_{mn}^{(1)} - M_{mn}^{(0)}M_{mn}^{(0)}$$

$$B_1 \equiv M_{mn}^{(-1)}M_{mn}^{(2)} - M_{mn}^{(0)}M_{mn}^{(1)}$$

$$B_2 \equiv M_{mn}^{(0)}M_{mn}^{(2)} - M_{mn}^{(1)}M_{mn}^{(1)}$$

#### IV. OUR ENERGY MODEL

Our energy model is the one-pole model of (26). Inserting (2) and (37) into (27),  $E$  in (26) is approximated by

$$E_1 \equiv \sum_{m=1}^M \sum_{n=1}^M \sum_{a=1}^{w_m} \sum_{b=1}^{w_n} \frac{1}{2} \tilde{C}_{mn} e^{-|t_m^a - t_n^b|/\tau_{mn}} \Delta V_m^a \Delta V_n^b \quad (38)$$

where  $m(n)$  is the label of interconnect,  $M$  is the number of the interconnects,  $a(b)$  is the label of event on root  $m(n)$ ,  $w_m(w_n)$  is the number of the events on root  $m(n)$ ,  $\tilde{C}_{mm}$  is the load capacitance of interconnect  $m$ ,  $|\tilde{C}_{mn}|$  ( $m \neq n$ ) is the coupling capacitance between interconnects  $m$  and  $n$ ,  $t_m^a(t_n^b)$  is the time of event  $a(b)$  on root  $m(n)$ ,  $\Delta V_m^a(\Delta V_n^b)$  is the change of the root voltage due to event  $a(b)$  on root  $m(n)$ , and

$$\tau_{mn} \equiv \frac{M_{mn}^{(0)}}{\tilde{C}_{mn}} \quad (39)$$

where  $M_{mn}^{(0)}$  is defined in (33).  $\tau_{mn}$  represents the correlation time length between two events on interconnects  $m$  and  $n$ , whose computation will be explained in more detail in Section V. Specifically, when  $m = n$ ,  $\tau_{mn}$  represents the time to charge/discharge interconnect  $m$ . In this sense,  $\tau_{mn}$  is called the *charge time* even when  $m \neq n$ . The energy model (38) is called the *E1 model* in this paper.

Note that the E1 model considers the coupling effects since each term depends on two events  $(m, a)$  and  $(n, b)$ , where  $(m, a)$  ( $(n, b)$ ) denotes event  $a$  ( $b$ ) on root  $m$  ( $n$ ). The term  $m \neq n$  ( $m = n$  but  $a \neq b$ ) is due to the mutual (self) coupling effects.

Ignoring terms representing the coupling effects in (38) (i.e., leaving terms such that  $(m, a) = (n, b)$ ), the following  $(1/2)CV^2$  model is obtained:

$$E_C = \sum_{m=1}^M \sum_{a=1}^{w_m} \frac{1}{2} \tilde{C}_{mm} (\Delta V_m^a)^2. \quad (40)$$

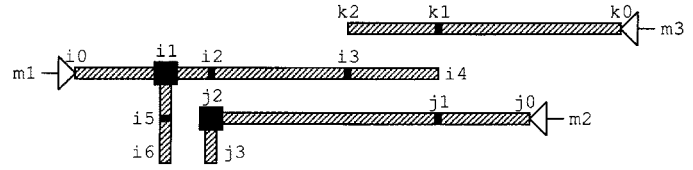


Fig. 7. Uniform segments.

In this paper, the energy model (40) is called the *EC model*. The following examples show the difference between the E1 and EC model.

In the first example, we assume  $M = 1$  and  $w_1 = 2$  as illustrated in Fig. 2(c). In this case

$$E_1 = \tilde{C}_{11} V_{DD}^2 (1 - e^{-\epsilon/\tau_{11}}), \quad E_C = \tilde{C}_{11} V_{DD}^2.$$

The term  $e^{-\epsilon/\tau_{11}}$  represents the self-coupling effects.

In the second example, we assume  $M = 2$  and  $w_1 = w_2 = 1$  as illustrated in Fig. 2(a) or (b). In this case

$$E_1 = \frac{1}{2} \left( \tilde{C}_{11} + \tilde{C}_{22} \pm 2|\tilde{C}_{12}|e^{-\epsilon/\tau_{12}} \right) V_{DD}^2 \quad (41)$$

where  $+$  ( $-$ ) sign is taken when  $\Delta V_1^1 = -\Delta V_2^1$  ( $\Delta V_1^1 = \Delta V_2^1$ ). On the other hand

$$E_C = \frac{1}{2} (\tilde{C}_{11} + \tilde{C}_{22}) V_{DD}^2$$

does not show any difference between these two cases. The factor  $e^{-\epsilon/\tau_{12}}$  represents the mutual coupling effects.

Using (18), (41) is also expressed as

$$E_1 = \frac{1}{2} \left( \tilde{\Gamma}_{11} + \tilde{\Gamma}_{22} + 2\tilde{\Gamma}_{12} \left( 1 \pm e^{-\epsilon/\tau_{12}} \right) \right) V_{DD}^2.$$

The term  $\tilde{\Gamma}_{12}(1 \pm e^{-\epsilon/\tau_{12}})$  is considered as the effective coupling capacitance. When  $\epsilon = 0$ , this effective coupling capacitance is either two or zero times of the original coupling capacitance  $\tilde{\Gamma}_{12}$ . This represents the Miller effects.

#### V. CALCULATION OF CHARGE TIME

This section presents an algorithm to calculate the charge time  $\tau_{mn}$  for the interconnects implemented by horizontal or vertical wires as shown in Fig. 7. We assume the via resistance and capacitance can be ignored and only adjacent parallel wires have coupling capacitance.

Each wire is divided into a minimum number of *uniform segments* such that the unit-length resistance, ground, and coupling capacitance are constant within each uniform segment. In Fig. 7,  $(j_0, j_2)$  is divided into two uniform segments,  $(j_0, j_1)$  and  $(j_1, j_2)$ . This is because the unit-length coupling capacitance is different for these two segments.

To apply our interconnect model, each uniform segment is further decomposed into small pieces of wire segments, each of which is considered as a discrete lumped electrical element as shown in Fig. 8. A piece of wire segment of length  $dx$  is represented by an edge, and the wire capacitance of the edge is assigned to junctions, which are represented by nodes in our interconnect graph.

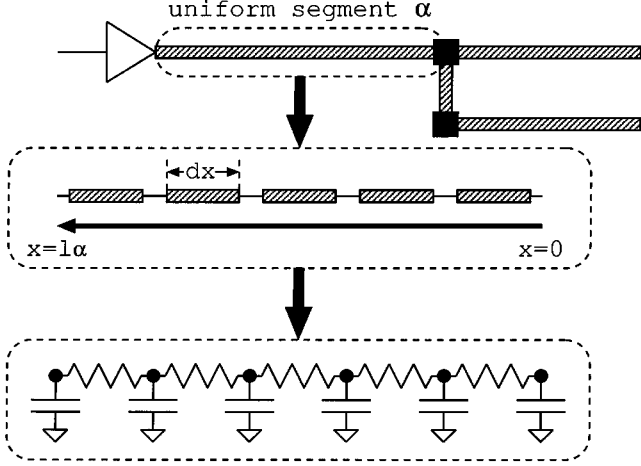


Fig. 8. Decomposition of a uniform segment.

To calculate  $\tau_{mn}$  defined by (39),  $\tilde{C}_{mn}$  and  $M_{mn}^{(0)}$  must be calculated for  $m, n = 1, \dots, M$ . According to (33)

$$M_{mn}^{(0)} = \sum_{i=1}^N R_{ii} \tilde{C}_{im} \tilde{C}_{in}. \quad (42)$$

Hence, we have to calculate  $\tilde{C}_{im}$  ( $i = 1, \dots, N$ ;  $m = 1, \dots, M$ ). According to (17),  $\tilde{C}_{im}$  is expressed as follows:

$$\tilde{C}_{im} = \sum_{w \in \mathcal{V}_m} C_{h(i), w} + \sum_{j \in \text{Child}(i)} \tilde{C}_{jm} \quad (43)$$

where  $h(i)$  is the head of edge  $i$ ,  $\mathcal{V}_m$  is the set of the nodes in interconnect  $m$  except its root, and  $\text{Child}(i)$  is the set of the edges outgoing from  $h(i)$  (cf. Fig. 6). Equation (43) shows that  $\tilde{C}_{im}$  can be calculated from the bottom up.

In the continuous limit  $dx \rightarrow 0$ , edge  $i$  is replaced by a point  $(\alpha, x)$ , where  $\alpha$  is a uniform segment, and  $x$  is the distance from the head of  $\alpha$  as shown in Fig. 8. Correspondingly,  $\tilde{C}_{im}$  ( $i = 1, \dots, N$ ;  $m = 1, \dots, M$ ) is replaced by  $\tilde{C}_{\alpha m}(x)$ , which is defined by

$$\tilde{C}_{\alpha m}(x) \equiv g_{\alpha m} x + \sum_{\beta \in \text{Child}(\alpha)} \tilde{C}_{\beta m}(l_{\beta}) \quad (44)$$

where  $\text{Child}(\alpha)$  is the set of the uniform segments outgoing from the head of  $\alpha$ ,  $l_{\beta}$  is the length of  $\beta$ , and

$$g_{\alpha m} \equiv \sum_{i=0}^2 \tilde{c}_{\alpha}^i \delta_{m, m_{\alpha}^i}$$

in which  $\delta_{m, m_{\alpha}^i}$  is the Kronecker delta,<sup>5</sup>  $m_{\alpha}^0$  is the label of the interconnect containing  $\alpha$ ,  $m_{\alpha}^1$  ( $m_{\alpha}^2$ ) is the label of the interconnect containing the upper/left (lower/right) adjacent wire, and

$$\tilde{c}_{\alpha}^i \equiv \begin{cases} \sum_{j=0}^2 \gamma_{\alpha}^j & (i=0), \\ -\gamma_{\alpha}^i & (i=1, 2), \end{cases}$$

where  $\gamma_{\alpha}^0$  is the unit-length ground capacitance of uniform segment  $\alpha$ , and  $\gamma_{\alpha}^1$  ( $\gamma_{\alpha}^2$ ) is the unit-length coupling capacitance between  $\alpha$  and the upper/left (lower/right) wire.

In the continuous limit, (42) is also replaced by

$$M_{mn}^{(0)} = \sum_{\alpha} \int_0^{l_{\alpha}} dx r_{\alpha} \tilde{C}_{\alpha m}(x) \tilde{C}_{\alpha n}(x) \quad (45)$$

<sup>5</sup> $\delta_{i,j} = 1$  for  $i = j$ , and  $\delta_{i,j} = 0$  for  $i \neq j$ .

where  $r_{\alpha}$  is the unit-length resistance of uniform segment  $\alpha$ . Note that the summation over  $i$  in (42) is replaced by the summation of the integrals over each uniform segment  $\alpha$  in (45). Also note that  $R_{ii}$  is replaced by  $r_{\alpha} dx$ .

Inserting (44) into (45), we obtain

$$M_{mn}^{(0)} = \sum_{\alpha} r_{\alpha} l_{\alpha} \left( \tilde{C}_{\alpha m} \left( \frac{l_{\alpha}}{2} \right) \tilde{C}_{\alpha n} \left( \frac{l_{\alpha}}{2} \right) + \frac{g_{\alpha m} g_{\alpha n} l_{\alpha}^2}{12} \right).$$

Based on the above arguments, the algorithm to calculate  $\tilde{C}_{mn}$  and  $M_{mn}^{(0)}$  is presented as follows:

Algorithm calcCM( $\alpha$ )

1.  $\vec{y} := 0$ ,  $\vec{z} := 0$ ;
2. **for** ( $\beta \neq \text{Child}(\alpha)$ )  $\vec{y} := \vec{y} + \text{calcCM}(\beta)$ ;
3. **for** ( $i = 0, 1, 2$ )  $z_{m_{\alpha}^i} + \tilde{c}_{\alpha}^i l_{\alpha} / 2$ ;
4.  $\vec{y} := \vec{y} + \vec{z}$ ;
5. **for** (each pair  $m, n$  such that  $y_m \neq 0$ ,  $y_n \neq 0$ )
6. **begin**
7.  $M_{mn}^{(0)} := M_{mn}^{(0)} + r_{\alpha} l_{\alpha} (y_m y_n + (1/3) z_m z_n)$ ;
8. **end**
9. **return**  $\vec{y} + \vec{z}$ ;

where  $\vec{y}$  ( $\vec{z}$ ) is a linked list with at most  $M$  entries, and  $y_m$  ( $z_m$ ) represents the entry of  $\vec{y}$  ( $\vec{z}$ ) corresponding to interconnect  $m$ . Before the first call of calcCM,  $M_{mn}^{(0)}$  is set at zero. Each step of calcCM is described as follows: At Line 2,  $y_m$  becomes  $y_m = \tilde{C}_{\alpha m}(0)$ . At Line 3,  $z_m$  becomes  $z_m = g_{\alpha m} l_{\alpha} / 2$ .  $y_m$  becomes  $\tilde{C}_{\alpha m}(l_{\alpha} / 2)$  (Line 4). The contribution from  $\alpha$  is added to  $M_{mn}^{(0)}$  (Lines 5–8). Finally,  $\tilde{C}_{\alpha m}(l_{\alpha})$  is returned (Line 9). By calling calcCM for all the roots, we obtain  $\tilde{C}_{mn}$  and  $M_{mn}^{(0)}$  for  $m, n = 1, \dots, M$ .

The time complexity of the algorithm is  $\mathcal{O}(MK^3)$ , where  $K$  is the maximum number of the uniform segments contained in one interconnect. The reason is as follows:  $\vec{y}$  has at most  $2K + 1$  nonzero elements since the number of the downstream uniform segments is at most  $K$ , each of them couples with at most two interconnects, and “1” represents the self-coupling. Hence, the time complexity of the **for** loop of Line 5–8 is  $\mathcal{O}(K^2)$ . Since this **for** loop is done at most  $MK$  times, the total time complexity is  $\mathcal{O}(MK^3)$ . Note that  $K$  is a function of the wire congestion and the maximum wire length driven by a driver. This means  $K$  is a local parameter and is independent of the circuit size  $M$ . Hence, the time complexity of our algorithm is  $\mathcal{O}(M)$  with respect to the circuit size.

## VI. EVENT-DRIVEN ENERGY CALCULATION

Because of four summation symbols in (38), straightforward calculation of  $E_1$  requires  $\mathcal{O}(M^2 w_{\max}^2)$  operations, where  $w_{\max} \equiv \max(w_1, \dots, w_M)$ . This section proposes a more efficient algorithm.

Our algorithm is based on the event-driven calculation, in which the increase of the energy due to each event is accumulated to obtain the total energy. In the  $(1/2)CV^2$  model, this procedure can be easily done by counting the number of events

<sup>6</sup>When edge  $i$  represents an output resistance, the above replacement is unnecessary since edge  $i$  is considered as a lumped electrical element.

and multiplying it by  $(1/2)CV^2$ . However, the consideration of coupling effects makes the procedure more complex.

The increase of the energy due to each event is obtained as follows. Assume that  $w_n$  events have already occurred on root  $n$  ( $= 1, \dots, M$ ) until the current time  $t$ . The total energy until now is equal to  $E_1$  given by (38). Let  $(m, a)$  denote a new event, which satisfies  $t_m^a \geq t_n^b$  for any other event  $(n, b)$ . Let  $E_1'$  denote the interconnect energy including event  $(m, a)$ , which is not included in  $E_1$ . The increase of the energy due to event  $(m, a)$  is equal to the difference  $\Delta E_m^a \equiv E_1' - E_1$ , which is expressed as

$$\Delta E_m^a = \frac{\tilde{C}_{mm} (\Delta V_m^a)^2}{2} + \sum_{n=1}^M \tilde{C}_{mn} e^{-(t_m^a - t_n^{w_n})/\tau_{mn}} X_{mn}^{w_n} \Delta V_m^a \quad (46)$$

where

$$X_{mn}^b = \sum_{c=1}^b e^{-(t_n^b - t_n^c)/\tau_{mn}} \Delta V_n^c. \quad (47)$$

Comparing (47) with

$$X_{mn}^{b-1} \equiv \sum_{c=1}^{b-1} e^{-(t_n^{b-1} - t_n^c)/\tau_{mn}} \Delta V_n^c$$

we obtain

$$X_{mn}^b = \begin{cases} 0, & (b = 0) \\ \Delta V_n^b + e^{-(t_n^b - t_n^{b-1})/\tau_{mn}} X_{mn}^{b-1}, & (b \geq 1). \end{cases} \quad (48)$$

Equations (46) and (48) lead us to the following event-driven energy calculation algorithm:

Algorithm calcE1()

1.  $E_1 := 0$ ;
2. **for** (each  $m$ )  $t_m := 0$ ;
3. **for** (each  $m, n$  such that  $\tilde{C}_{mn} \neq 0$ )  $X_{mn} := 0$ ;
4. Set up event queue  $EQ$ ;
5. **while** ( $EQ$  is not empty)
6. **begin**
7. Pop the first event  $(m, a)$  from  $EQ$ ;
8.  $E_1 := E_1 + (1/2)\tilde{C}_{mm} (\Delta V_m^a)^2$ ;
9. **for** (each  $n$  such that  $\tilde{C}_{mn} \neq 0$ )
10. **begin**
11.  $E_1 := E_1 + \tilde{C}_{mn} e^{(t_n - t_m^a)/\tau_{mn}} X_{mn} \Delta V_m^a$ ;
12.  $X_{nm} := \Delta V_m^a + e^{(t_m - t_m^a)/\tau_{nm}} X_{nm}$ ;
13. **end**
14.  $t_m := t_m^a$ ;
15. **end**

in which  $E_1$ ,  $t_m$ , and  $X_{mn}$  are initialized (Lines 1, 2, 3), the events are ordered and stored in the event queue  $EQ$  (Line 4), the earliest event in  $EQ$  is retrieved and removed from  $EQ$  (Line 7), the self-component of the energy is added to  $E_1$  (Line 8), the coupling components of the energy are added to  $E_1$  (Line 11),  $X_{nm}$  is updated for the next calculation (Line 12), and  $t_m$  is updated (Line 14).

Note that the above algorithm only needs the latest event on each root, and we can discard older events. This means our al-

gorithm can be implemented on an event-driven logic simulator such as Verilog-XL.

The time complexity of the algorithm is  $\mathcal{O}(WK)$ , where  $W = \sum_{m=1}^M w_m$  is the number of the events.  $\mathcal{O}(K)$  comes from **for** loop of Line 9–13 since the number of  $n$  such that  $\tilde{C}_{mn} \neq 0$  is at most  $2K + 1$  as shown in Section V. Since  $K$  is independent of  $W$ , the time complexity with respect to  $W$  is  $\mathcal{O}(W)$ , which is also that of the event-driven simulation without energy calculation. This means our algorithm does not change the time complexity of the event-driven simulation.

## VII. ENERGY AND SIGNAL CORRELATION

This section shows that the energy from mutual coupling can be ignored if the signals on the coupling interconnects are mutually independent. This leads to the further speedup of the algorithms proposed in Sections V and VI.

### A. Cancellation of Energy

To explain the relation between interconnect energy and signal correlation, we start with a simple example shown in Fig. 2(a) and (b), in which  $(m, a)$  and  $(n, b)$  form an  $\epsilon$ -aligned pair, and  $(m, c)$  and  $(n, d)$  form an  $\epsilon$ -antialigned pair, where the  $\epsilon$ -aligned ( $\epsilon$ -antialigned) pair is the event pair switching in the same (opposite) direction with time difference  $\epsilon$ . To calculate the contributions to  $E_{mn}$  from these pairs, we insert (2) into (27) to obtain

$$E_{mn} = \sum_{a=1}^{w_m} \sum_{b=1}^{w_n} \frac{1}{2} H_{mn}(|t_m^a - t_n^b|) \Delta V_m^a \Delta V_n^b.$$

According to this equation, the contribution to  $E_{mn}$  from the  $\epsilon$ -aligned pair  $((m, a), (n, b))$  is  $H_{mn}(\epsilon) \Delta V_m^a \Delta V_n^b$  while that from the  $\epsilon$ -antialigned pair  $((m, c), (n, d))$  is  $H_{mn}(\epsilon) \Delta V_m^c \Delta V_n^d$ . These contributions cancel each other out since  $\Delta V_m^c = \Delta V_m^a$  and  $\Delta V_n^d = -\Delta V_n^b$ .

In general,  $E_{mn} = 0$  when the number of the  $\epsilon$ -aligned pairs is equal to that of the  $\epsilon$ -antialigned pairs for any  $\epsilon$ . The number of the  $\epsilon$ -aligned pairs is equal to that of the  $\epsilon$ -antialigned pairs when  $V_m$  and  $V_n$  are mutually independent. This is because when  $V_m$  and  $V_n$  are mutually independent, the signals of  $V_m$  and  $V_n$  can switch independently, and the probability of the appearance of an  $\epsilon$ -aligned pair is equal to that of an  $\epsilon$ -antialigned pair. In summary, we have the following.

*Theorem 1:*  $E_{mn} \approx 0$  if  $V_m$  and  $V_n$  are independent.

Before proving Theorem 1, the meanings of the statements “ $E_{mn} \approx 0$ ” and “ $V_m$  and  $V_n$  are independent” must be made clear.

To explain “ $E_{mn} \approx 0$ ,” we modify (27) to obtain

$$E_{mn} = \lim_{T \rightarrow \infty} E_{mn}(T)$$

where

$$E_{mn}(T) \equiv \frac{I_{mn}(T) + I_{nm}(T)}{2}$$

$$I_{mn}(T) \equiv \int_0^\infty d\epsilon H_{mn}(\epsilon) \int_0^T d\xi \dot{V}_m(\xi) \dot{V}_n(\xi + \epsilon)$$

and we used (29). “ $E_{mn} \approx 0$ ” means

$$\lim_{T \rightarrow \infty} \frac{E_{mn}(T)}{T} = 0.$$

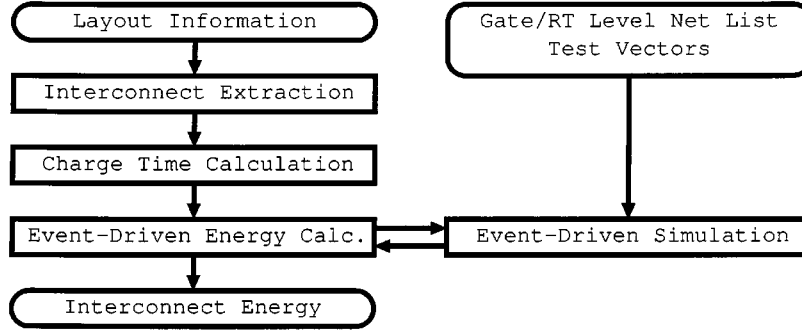


Fig. 9. Interconnect energy calculation flow.

Roughly speaking, this means the average power is zero since  $E_{mn}(T)$  is a component of the energy due to events up to time  $T$ , and  $\lim_{T \rightarrow \infty} E_{mn}(T)/T$  is the average power.

To explain “ $V_m$  and  $V_n$  are independent,” we introduce the average of a signal and a signal pair. The average of  $V_m$ , denoted by  $\langle V_m \rangle$ , is defined by the following time average:

$$\langle V_m \rangle \equiv \lim_{T \rightarrow \infty} \frac{1}{T} \int_0^T d\xi V_m(\xi).$$

Similarly, the average of  $V_m(\xi)V_n(\xi + \epsilon)$  is defined by

$$\langle V_m(\xi)V_n(\xi + \epsilon) \rangle \equiv \lim_{T \rightarrow \infty} \frac{1}{T} \int_0^T d\xi V_m(\xi)V_n(\xi + \epsilon).$$

$\langle V_m(\xi)V_n(\xi + \epsilon) \rangle$  represents the signal correlation between  $V_m$  and  $V_n$ . In this paper, “ $V_m$  and  $V_n$  are independent” means  $\langle V_m(\xi)V_n(\xi + \epsilon) \rangle = \langle V_m \rangle \langle V_n \rangle$  holds for all  $\epsilon$ .

Using above definitions, Theorem 1 is proved as follows.

*Proof:* It is enough to show

$$P_{mn} \equiv \lim_{T \rightarrow \infty} \frac{I_{mn}(T)}{T} = 0$$

when  $V_m$  and  $V_n$  are independent. In this case

$$\begin{aligned} P_{mn} &= \int_0^\infty d\epsilon H_{mn}(\epsilon) \langle \dot{V}_m(\xi)\dot{V}_n(\xi + \epsilon) \rangle \\ &= \int_0^\infty d\epsilon H_{mn}(\epsilon) \langle \dot{V}_m \rangle \langle \dot{V}_n \rangle. \end{aligned}$$

Since  $V_m$  is bounded ( $0 \leq V_m \leq V_{DD}$ )

$$\langle \dot{V}_m \rangle = \lim_{T \rightarrow \infty} \frac{1}{T} \int_0^T d\xi \dot{V}_m(\xi) = \lim_{T \rightarrow \infty} \frac{V_m(T) - V_m(0)}{T} = 0.$$

Therefore,  $P_{mn} = 0$ . ■

### B. Energy Model Without Signal Correlation

Assume that  $V_m$  and  $V_n$  are independent for each coupled pair  $m$  and  $n$ . In other words

$$\tilde{C}_{mn}(m \neq n) \neq 0 \implies V_m \text{ and } V_n \text{ are independent.}$$

In this case, according to Theorem 1 we can ignore  $E_{mn}$  ( $m \neq n$ ) in (38) and obtain the following new model:

$$E_0 = \sum_{m=1}^M \sum_{a=1}^{w_m} \sum_{b=1}^{w_m} \frac{1}{2} \tilde{C}_{mm} e^{-|t_m^a - t_m^b|/\tau_{mm}} \Delta V_m^a \Delta V_m^b. \quad (49)$$

The interconnect energy model given by (49) is called the *E0 model* in this paper. The E0 model is faster than the E1 model since the calculation for  $E_{mn}$  ( $m \neq n$ ) is omitted. In fact, Line 5 of calcCM in Section V is replaced by

for(each  $m$  such that  $y_m \neq 0$ )

and the time complexity of calcCM becomes  $\mathcal{O}(MK^2)$ . Also, calcE1 in Section VI is replaced by Algorithm calcE0().

Algorithm calcE0()

1.  $E_0 := 0$ ;
2. **for** (each  $m$ )  $t_m := 0$ ,  $X_m := 0$ ;
3. Set up event queue  $EQ$ ;
4. **while** ( $EQ$  is not empty)
5.     **begin**
6.         Pop the first event  $(m, a)$  from  $EQ$ ;
7.          $X_m := \Delta V_m^a + e^{(t_m - t_m^a)/\tau_{mm}} X_m$
8.          $E_0 := E_0 + \tilde{C}_{mm}(X_m - (1/2)\Delta V_m^a)\Delta V_m^a$ ;
9.          $t_m := t_m^a$ ;
10.     **end**

The time complexity of calcE0 is  $\mathcal{O}(W)$ .

## VIII. SUMMARY OF OUR ENERGY MODEL

Since our interconnect energy model requires interconnect topology and geometry, it is most useful in an interconnect-centric design flow described in [1]. Our interconnect energy model can be applied at any design stage in the above design flow such as the interconnect planning level with floorplanning, interconnect synthesis level, and interconnect layout including detail routing. In any of these design stages, the interconnect energy estimation is basically composed of the following three steps:

- 1) interconnect extraction;
- 2) charge time calculation;
- 3) event-driven energy calculation.

Procedure 1 includes the extraction of the unit-length resistance, ground, and coupling capacitance for each uniform segment after decomposing interconnects in a sequence of uniform segments. In Procedures 2 and 3, we use the algorithms presented in Section V and VI, respectively. Procedure 3 can be efficiently performed with any commercially available event-driven logic simulator, such as Verilog-XL/PLI. The above procedures are illustrated in Fig. 9.

TABLE I  
COMPARISON OF INTERCONNECT ENERGY MODELS

model	complexity	condition/assumption
EC	$MK + W$	Coupling effects are not considered.
E0	$MK^2 + W$	Only self coupling effects are considered. One-pole model.
E1	$MK^3 + WK$	Mutual and self coupling effects are considered. One-pole model.

TABLE II  
COMPARISON OF ERROR AND RUNTIME

circuit	error (%)			runtime (sec.)			
	EC	E0	E1	EC	E0	E1	HSPICE
c(10,10)	76	2.4	0.6	.00	.00	.01	70
c(10,20)	76	-0.5	1.0	.00	.01	.01	190
c(10,30)	88	3.3	3.0	.00	.01	.01	560
c(20,10)	73	1.6	1.0	.00	.01	.02	300
c(20,20)	90	2.7	2.4	.00	.01	.05	1600
c(20,30)	94	4.6	3.9	.00	.02	.05	4800
c(30,10)	77	3.1	1.7	.00	.00	.04	910
c(30,20)	89	3.8	3.3	.01	.01	.08	6200
c(30,30)	93	4.0	3.8	.00	.01	.10	27000
c(1000,10)	-	-	-	.02	.12	2.5	-
c(5000,10)	-	-	-	.06	.55	13	-
c(10 <sup>4</sup> ,10)	-	-	-	.18	1.2	27	-

Table I compares the interconnect energy models described in this paper, where “complexity” is the sum of the complexities for Procedures 2 and 3.

## IX. EXPERIMENTAL RESULTS

We implemented our algorithm to compare it with HSPICE on a SUN ULTRA 60 workstation running at 360 MHz. We used the 70-nm CMOS technology derived in [10] in our test, where the clock frequency is 1 GHz and  $V_{DD} = 0.75$  V. We assumed minimum wire width and spacing, in which ground capacitance is  $0.054f$  F/ $\mu\text{m}$ , coupling capacitance is  $0.119f$  F/ $\mu\text{m}$ , and resistance is  $0.36 \Omega/\mu\text{m}$  for a unit-length wire. The unit-length inductance is assumed to be  $1$  pH/ $\mu\text{m}$ .

In Table II,  $c(M, L)$  represents a circuit with  $M$  interconnects, each of which has  $L$  edges. In this case,  $N = M \times L$ . The topology of the circuit is randomly generated such that each edge has 0–3 children, and couples with 1 or 2 edges. Note that such a topology may not correspond to a real layout. The wire length is determined such that the maximum Elmore delay is less than half of the clock cycle. Each interconnect is driven by a CMOS driver with output resistance  $32.7 \Omega$  and gate capacitance  $23.1f$  F, which is also considered to be the sink capacitance. Each input waveform is randomly generated. In addition to the “proper” events (expected events by the functionality of the circuit), we also include the “glitch” events (unexpected events, noise). The time interval between a glitch event and the nearest event, which is either proper or glitch event, is 40–120 ps. Input waveforms have a length of 50 clock cycles and are mutually independent.

Columns 2–4 of Table II, labeled EC, E0, and E1, show the estimation error of the energy compared with HSPICE for EC, E0, and E1 models, respectively. The missing entries “-” are

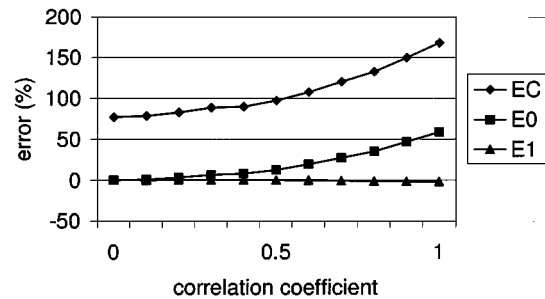


Fig. 10. Relation between error and correlation coefficient.

due to too long HSPICE runtime. The total energy, including CMOS driver energy, is measured by HSPICE using the “POWER” command as the basis for comparison. The total energy values for EC, E0, and E1 are computed as the sum of the interconnect energy estimated by each model, and the total estimated driver internal energy using (7) in Section II-E.

The results show that our models (E0 and E1 models) are within 5% accuracy of HSPICE, while the error of the commonly used  $(1/2)CV^2$  model (EC model) can be as large as 94%.

In Table II, there is no obvious difference between E0 and E1 since the signals are mutually independent. Fig. 10 shows the relation between error and signal correlation for  $c(10,10)$ . The vertical axis represents the error compared with HSPICE, and the horizontal axis represents the average *correlation coefficient* between two roots. The correlation coefficient between roots  $m$  and  $n$  is defined by  $r_{mn} \equiv |p_{mn} - p_m p_n| / \sqrt{p_m(1-p_m)p_n(1-p_n)}$ , where  $p_m$  is the probability of  $V_m$  being  $V_{DD}$ , and  $p_{mn}$  is the probability of  $V_m$  and  $V_n$  being simultaneously  $V_{DD}$ . The value  $r_{mn} = 0$  implies  $V_m$  and  $V_n$  are mutually independent, and  $r_{mn} = 1$  implies they are maximally correlated, i.e., either  $V_m \equiv V_n$  or  $V_m \equiv V_{DD} - V_n$ . According to Fig. 10, the error of E0 is large when the correlation is strong. This is consistent with our analysis in Section VII.

Columns 5–8 of Table II compare the runtime where “.00” means “less than 0.01.” The overhead to read in SPICE files is excluded for EC, E0, and E1 since it is negligible compared with HSPICE runtime. The results for large circuits  $c(1000,10)$ ,  $c(5000,10)$ ,  $c(10000,10)$ , show the runtime of EC, E0, E1 to be linear with respect to the circuit size.

The above results show that the following hybrid approach would be efficient: EC is used for short interconnects, E0 is used for long interconnects, and  $E_{mn}$  ( $m \neq n$ ) is added if the signals at roots  $m$  and  $n$  are strongly correlated. The strength of the correlation is represented by  $r_{mn}$ , which can be obtained using a probabilistic approach [11]–[13].

## X. ONGOING FUTURE WORKS

### A. Stability Analysis

Although the exact  $H_{mn}(t)$  is stable as shown in (31), the stability for the one-pole model is not guaranteed. According to (37) and (39), the stability condition for the one-pole model is  $\tau_{mn} > 0$ .

This stability condition is guaranteed when  $m = n$  since  $\tau_{mm} = \sum_{i=1}^N R_{ii} \tilde{C}_{im}^2 / \tilde{C}_{mm}$  is positive (cf.  $\tilde{C}_{mm} > 0$ ).

On the other hand,  $\tau_{mn} = \tau_{mn}^{(0)} - \tau_{mn}^{(1)}$  for  $m \neq n$ , where

$$\tau_{mn}^{(0)} \equiv \sum_{i \in \mathcal{E}_m \cup \mathcal{E}_n} \frac{R_{ii} |\tilde{C}_{im} \tilde{C}_{in}|}{|\tilde{C}_{mn}|}$$

$$\tau_{mn}^{(1)} \equiv \sum_{i \notin \mathcal{E}_m \cup \mathcal{E}_n} \frac{R_{ii} |\tilde{C}_{im} \tilde{C}_{in}|}{|\tilde{C}_{mn}|}$$

in which  $\mathcal{E}_m$  is the set of the edges in interconnect  $m$ , and we used the fact that  $\tilde{C}_{im} \geq 0$  when  $i \in \mathcal{E}_m$ , and  $\tilde{C}_{im} \leq 0$  when  $i \notin \mathcal{E}_m$ , obtained by (3) and (17). Note that the one-pole model is unstable when  $\tau_{mn}^{(0)} < \tau_{mn}^{(1)}$ .

To overcome this difficulty, we replace the negative  $\tau_{mn}$  with zero. In this case,  $E_{mn} = 1/2 \tilde{C}_{mn} V_{DD}^2 (w_{mn}^{(0)} - w_{mn}^{(1)})$ , where  $w_{mn}^{(0)}$  ( $w_{mn}^{(1)}$ ) is the number of the simultaneous transitions switching in the same (opposite) direction. We ignore  $w_{mn}^{(0)}$  and  $w_{mn}^{(1)}$  since the simultaneous transition rarely occurs. This means  $E_{mn}$  can be ignored when  $\tau_{mn} < 0$ .

Although the above prescription (i.e., replacing negative  $\tau_{mn}$  with zero) works well in our experimental results, further research would be required.

### B. Event Propagation

As described in Section VIII, the event propagation is the task for the event-driven simulator, but not for our energy models or the  $(1/2)CV^2$  model. However, it is important to investigate the event propagation with consideration of coupling effects. For example, in Fig. 2(c), the input pulse of width  $\epsilon$  becomes smaller pulses at sinks  $v_1$  and  $v_2$  due to self-coupling. If we assume sinks  $v_1$  and  $v_2$  are also inputs of other gates with threshold voltage  $V_{DD}/2$ , then the pulse at node  $v_1$  is propagated through the gate while the pulse at node  $v_2$  is not. In other words, the pulse at node  $v_2$  disappears. In this paper, the disappearance of a pulse due to self coupling is called the *event evaporation*.

To consider event evaporation in the event propagation algorithm, we analyze the sink voltage (i.e., input of the next gate). Using the one-pole model for (20), the voltage of node  $v$  (i.e.,  $U_v$ ) in interconnect  $m$  is expressed as

$$U_v(t) = V_m(t) - e^{-(t-t_m^{w_m(t)})/d_{mv}} Y_{mv}^{w_m(t)} \quad (50)$$

where  $w_m(t)$  is the label of the last event before time  $t$

$$Y_{mv}^a = \begin{cases} 0, & (a = 0) \\ \Delta V_m^a + e^{-(t_m^a - t_m^{a-1})/d_{mv}} Y_{mv}^{a-1}, & (a \geq 1) \end{cases}$$

and  $d_{mv} \equiv \sum_{i \in Up(v)} R_{ii} \tilde{C}_{im}$  is the Elmore delay from root  $m$  to node  $v$ , where  $Up(v)$  denotes all the upstream edges of node  $v$ . Note that inductance and mutual coupling effects do not appear in (50).

The time when  $U_v$  crosses the threshold voltage is the solution of  $U_v(t) = V_{DD}/2$  and is expressed as

$$t = t_m^{w_m(t)} + d_{mv} \log \frac{2|Y_{mv}^{w_m(t)}|}{V_{DD}}$$

with the condition that

$$t_m^{w_m(t)} \leq t \leq t_m^{w_m(t)+1}. \quad (51)$$

Condition (51) means that event  $(m, w_m(t))$  must be propagated to the next gate at later time  $t$ , but before the next event  $(m, w_m(t) + 1)$ . If (51) is not satisfied, the event is not propagated due to event evaporation.

The above arguments lead to the following event propagation algorithm with consideration of event evaporation.

```

Algorithm eventPropagation()
1. for (each sink  $v$ )  $t_v := -1$ ,  $Y_v := 0$ ;
2. Set up event queue  $EQ$ ;
3. while ( $EQ$  is not empty)
4. begin
5. Pop the first event  $(m, a)$  from  $EQ$ ;
6. for (each sink  $v$  of interconnect  $m$ )
7. begin
8.  $Y_v := \Delta V_m^a + e^{-(t_m^a - t_m^{a-1})/d_{mv}} Y_v$ ;
9. if ( $t_v \geq 0$ )
10. begin
11. Delete event  $t_v$  from  $EQ$ ;
12.  $t_v := -1$ ;
13. end
14.  $t = t_m^a + d_{mv} \log(2|Y_v|/V_{DD})$ ;
15. if ( $t \geq t_m^a$ )
16. begin
17. Add event  $t$  to  $EQ$ ;
18.  $t_v := t$ ;
19. end
20. end
21. end

```

In this algorithm,  $t_v$  represents the time of the next event scheduled at node  $v$ , and  $t_v = -1$  means there is no scheduled event. Event evaporation is considered at Lines 9–13 to satisfy  $t \leq t_m^{w_m(t)+1}$ , and at Lines 15–19 to satisfy  $t_m^{w_m(t)} \leq t$ .

According to our preliminary experiments, the above algorithm is very accurate with the same time complexity as the conventional event-driven simulation. However, further investigation would be necessary to include mutual coupling.

### C. Resistive Shielding

In this section, we investigate the energy of a pulse propagated through an interconnect shown in Fig. 11.

When the length  $L$  of the interconnect is longer than certain critical length  $L_{\text{crit}}$ , the pulse disappears on the way to the other end of the interconnect due to the *resistive shielding effect*. This means the energy is a constant  $E_{\text{sat}}$  for  $L > L_{\text{crit}}$  since the pulse can charge/discharge only a definite part of the interconnect. The following questions arise.

- (Q1) Is our energy model accurate with the existence of the resistive shielding effect?
- (Q2) What is the value of  $L_{\text{crit}}$ ?
- (Q3) What is the value of  $E_{\text{sat}}$ ?

To answer these questions, we solve the following RC transmission line equations:

$$rI(t, x) = \frac{\partial V}{\partial x}(t, x), \quad c \frac{\partial V}{\partial t}(t, x) = \frac{\partial I}{\partial x}(t, x) \quad (52)$$

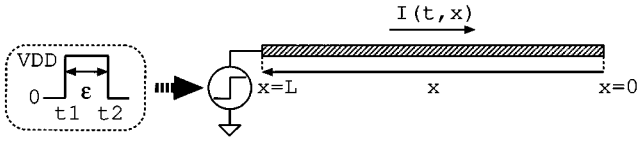


Fig. 11. RC Transmission line.

where  $t$  is the time,  $x$  is the distance from the far end of the interconnect,  $I(t, x)$  and  $V(t, x)$  are the current and voltage at  $x$  at time  $t$ , and  $r$  and  $c$  are the unit-length resistance and capacitance, respectively. We assume  $r = 0.36 \Omega/\mu\text{m}$  and  $c = 0.292 \text{ fF}/\mu\text{m}$ . The boundary condition is given by

$$V(t, x = L) = v(t), \quad I(t, x = 0) = I(t = 0, x) = 0 \quad (53)$$

where  $v(t)$  is the voltage waveform of the pulse, whose time derivative is expressed as

$$\dot{v}(t) = \sum_{a=1}^2 \delta(t - t_a) \Delta V_a.$$

The solution of (52) with (53) is

$$I(t, x) = \sum_{n=-\infty}^{\infty} (-1)^n I_n(t) \sin \left[ \left( \frac{\pi}{2} + n\pi \right) \frac{x}{L} \right] \quad (54)$$

where

$$I_n(t) \equiv \sum_{a=1}^2 \theta(t - t_a) \frac{\Delta V_a}{R} \exp \left[ -\frac{t - t_a}{RC} \left( \frac{\pi}{2} + n\pi \right)^2 \right]$$

in which  $R \equiv rL$  and  $C \equiv cL$  are the total resistance and capacitance, respectively. Inserting (54) into the definition of the energy

$$E_T = \int_0^{\infty} dt \int_0^L dx r(I(t, x))^2$$

we obtain

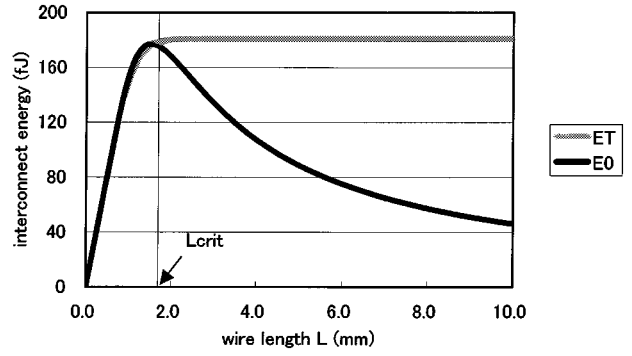
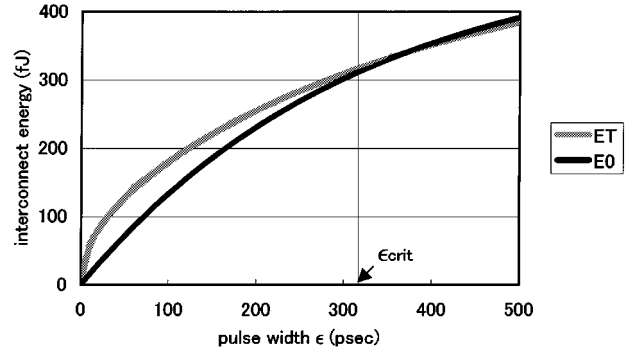
$$E_T = CV_{DD}^2 \sum_{n=-\infty}^{\infty} \frac{1 - \exp \left[ -\frac{\epsilon}{RC} \left( \frac{\pi}{2} + n\pi \right)^2 \right]}{\left( \frac{\pi}{2} + n\pi \right)^2}. \quad (55)$$

The energy model (55) is called the *ET model* in this section.

According to (39) and (45), the charge time for the RC transmission line is  $RC/3$ . Hence, *E0* model defined by (49) becomes

$$E_0 = CV_{DD}^2 \left( 1 - \exp \left[ -\frac{3\epsilon}{RC} \right] \right). \quad (56)$$

The energy given by *ET* and *E0* models is plotted in Figs. 12 and 13 as a function of the wire length and pulse width. Fig. 12 shows that  $E_T$  does not depend on the wire length when  $L > L_{\text{crit}}$  as conjectured at the beginning of this section. On the other hand,  $E_0$  is smaller than  $E_T$  when  $L > L_{\text{crit}}$ . However, this does not mean the *E0* model is inaccurate as will be explained in the following. In the real circuits, in addition to the pulse events, there are also full-swing events. The energy of a full-swing event (i.e.,  $(1/2)CV^2$ ) is proportional to  $L$  while that of a pulse event is constant when  $L > L_{\text{crit}}$ . This means the error of the pulse

Fig. 12. Comparison of *ET* and *E0* models as functions of wire length with fixed pulse width (100 ps).Fig. 13. Comparison of *ET* and *E0* models as functions of pulse width with fixed wire length (3 mm).  $\epsilon_{\text{crit}} \equiv RC/3$  is the charge time.

energy is not important compared with the full-swing energy when  $L > L_{\text{crit}}$ . In fact, Fig. 14 shows that the error of the normalized energy (i.e., the ratio of the pulse energy to the full-swing energy) of *E0* model is small. As a result, the answer to (Q1) is “YES”.

To answer (Q2), note that the charge time is the time to charge/discharge the interconnect. This means that when the pulse width  $\epsilon$  is larger than the charge time  $\tau$ , the interconnect is charged/discharged. When  $\epsilon < \tau$ , the interconnect is not completely charged/discharged, i.e., the resistive shielding effect appears when  $\epsilon < \tau$ . Hence,  $L_{\text{crit}}$  is the solution of  $\epsilon = \tau$ . Since  $\tau = RC/3$ , we obtain

$$L_{\text{crit}} = \sqrt{\frac{3\epsilon}{rc}}. \quad (57)$$

$L_{\text{crit}}$  in Figs. 12 and 14 is given by (57).

To answer (Q3), note that the energy is constant when  $L > L_{\text{crit}}$ . This means  $E_{\text{sat}} \approx E_T(L \rightarrow \infty)$ . Replacing  $1/L \sum_n$  with  $\int dx$ , and  $(n + 1/2)/L$  with  $x$ , in (55), we obtain

$$\begin{aligned} E_T(L \rightarrow \infty) &= \lim_{L \rightarrow \infty} \frac{CV_{DD}^2}{L^2} \\ &\times \sum_{n=-\infty}^{\infty} \frac{1 - \exp \left[ -\frac{\epsilon \pi^2}{rc} \left( \frac{n + \frac{1}{2}}{L} \right)^2 \right]}{\left( \frac{n + \frac{1}{2}}{L} \right)^2 \pi^2} \\ &= \frac{cV_{DD}^2}{\pi^2} \int_{-\infty}^{\infty} dx \frac{1 - \exp \left[ -\frac{\epsilon \pi^2}{rc} x^2 \right]}{x^2} \end{aligned}$$

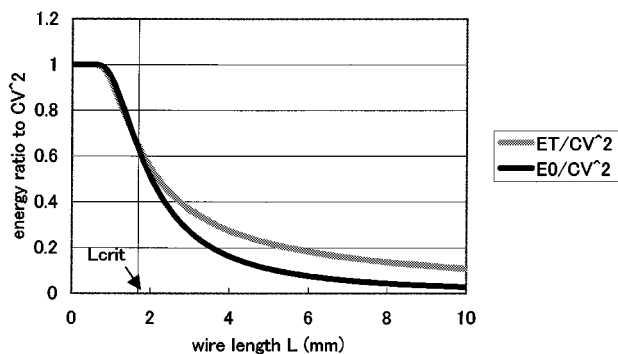


Fig. 14. Comparison of normalized energy for ET and  $E_0$  models as functions of wire length with fixed pulse width (100 ps).

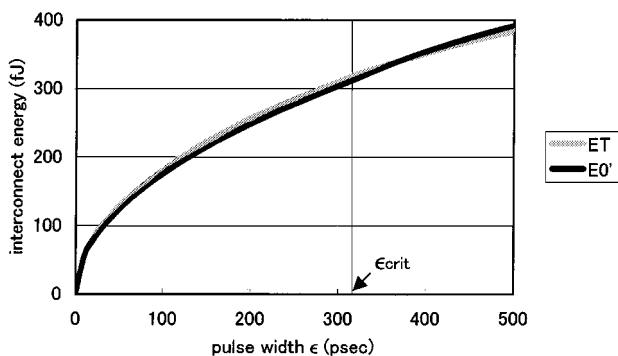


Fig. 15. Comparison of ET and  $E_0'$  models as functions of pulse width with fixed wire length (3 mm).  $\epsilon_{\text{crit}} \equiv RC/3$  is the charge time.

$$= 2V_{DD}^2 \sqrt{\frac{c\epsilon}{r\pi}}.$$

On the other hand, since  $E_0$  is a good approximation when  $L < L_{\text{crit}}$ ,  $E_{\text{sat}}$  can be also represented by  $E_0$  at  $L = L_{\text{crit}}$ . According to (56) and (57), we obtain

$$E_0(L_{\text{crit}}) = V_{DD}^2 \sqrt{\frac{3c\epsilon}{r}} (1 - e^{-1}).$$

Comparing  $E_T(L \rightarrow \infty)$  with  $E_0(L_{\text{crit}})$ , we obtain

$$\frac{E_0(L_{\text{crit}})}{E_T(L \rightarrow \infty)} = \frac{\sqrt{3\pi}}{2} (1 - e^{-1}) \approx 0.970298775.$$

This means  $E_0(L_{\text{crit}}) \approx E_T(L \rightarrow \infty)$  with less than 3% error. The important thing is that  $E_0(L_{\text{crit}})/E_T(L \rightarrow \infty)$  is a mathematical constant and is independent of any circuit parameters such as wire length and pulse width. As a result, the answer to (Q3) is that  $E_{\text{sat}}$  is *always* approximated by  $E_0(L_{\text{crit}})$ !

The above results imply that the accuracy of our energy model can be improved if we replace  $E_0$  with  $E_0(L_{\text{crit}})$  when  $L > L_{\text{crit}}$ . In the  $\epsilon$  domain, this means  $E_0$  is replaced with

$$E_0'(\epsilon) = \begin{cases} CV_{DD}^2 (1 - \exp[-\frac{3\epsilon}{RC}]) & (\epsilon \geq \frac{RC}{3}) \\ CV_{DD}^2 \sqrt{\frac{3c\epsilon}{r}} (1 - e^{-1}) & (\epsilon < \frac{RC}{3}) \end{cases}$$

where the first row is nothing but (56) and the second row is obtained by replacing  $L$  with  $L_{\text{crit}}$  defined by (57). Fig. 15 shows that  $E_0'$  is more accurate than  $E_0$  in Fig. 13.

In this section, we have shown a method to correct the error of our model for a simple circuit using  $L_{\text{crit}}$  and  $E_{\text{sat}}$ , which are

obtained by our model without using the solution of the transmission line equations. However, it is not obvious whether this method can be extended to more general circuits including coupling interconnects with more general topology. This is for future work.

## XI. CONCLUSION

This paper presented an interconnect energy model with consideration of coupling effects, such as crosstalk noise and incomplete voltage swing, which are significant for deep submicron design. Our interconnect energy model is characterized by a new parameter, called the charge time, which represents the correlation time length between two events. We developed an efficient algorithm to calculate the charge time and showed that its time complexity is linear with respect to the circuit size. We also developed an event-driven algorithm to calculate the interconnect energy and showed that its time complexity is also linear with respect to the number of events. Furthermore, we investigated the relationship between interconnect energy and signal correlation, and proposed a simplified model (i.e., (49)). Experimental results show that our approach is several orders of magnitude faster than HSPICE with less than 5% error. In comparison, the error of the  $(1/2)CV^2$  model can be as high as 100%.

Our future work will concentrate on the continued improvement of our energy model as discussed in Section X, and application to the power optimization at the global interconnect planning level.

## REFERENCES

- [1] J. Cong, "An interconnect-centric design flow for nanometer technologies," *Proc. IEEE*, vol. 89, pp. 505–528, Apr. 2001.
- [2] *National Technology Roadmap for Semiconductors*: Semiconductor Industry Assoc., 1997.
- [3] K.-W. Kim, S.-O. Jung, U. Narayanan, C. L. Liu, and S.-M. Kang, "Noise-aware power optimization for on-chip interconnect," in *Int. Symp. Low Power Electronics Design*, Italy, 2000, pp. 108–113.
- [4] M. Favalli and L. Benini, "Analysis of glitch power dissipation in CMOS IC's," in *Int. Symp. Low Power Electronics Design*, Laguna, CA, 1995, pp. 123–128.
- [5] D. Rabe and W. Nebel, "New approach in gate-level glitch modeling," in *Eur. Design Automation Conf.*, Paris, France, 1996, pp. 66–71.
- [6] M. Hashimoto, H. Onodera, and K. Tamaru, "A practical gate resizing technique considering glitch reduction for low power design," in *36th Design Automation Conf.*, New Orleans, LA, 1999, pp. 446–451.
- [7] T. Uchino and J. Cong, "An interconnect energy model considering coupling effects," in *38th Design Automation Conf.*, Las Vegas, NV, 2001, pp. 555–558.
- [8] —, "Interconnect energy model considering coupling effects," UCLA Computer Sci. Dept., 010003.
- [9] L. T. Pillage and R. A. Rohrer, "Asymptotic waveform evaluation for timing analysis," *IEEE Trans. Computer-Aided Design*, vol. 9, pp. 352–366, 1990.
- [10] J. Cong, L. He, K.-Y. Khoo, C.-K. Koh, and D. Z. Pan, "Interconnect design for deep submicron IC's," in *Int. Conf. Computer Aided Design*, San Jose, CA, 1997, pp. 478–485.
- [11] F. N. Najm, "Transition density, a stochastic measure of activity in digital circuits," in *28th Design Automation Conf.*, San Francisco, CA, 1991, pp. 644–649.
- [12] R. Marculescu, D. Marculescu, and M. Pedram, "Switching activity analysis considering spatiotemporal correlations," in *Int. Conf. Computer Aided Design*, San Jose, CA, 1994, pp. 294–299.
- [13] T. Uchino, F. Minami, T. Mitsuhashi, and N. Goto, "Switching activity analysis using boolean approximation method," in *Int. Conf. Computer Aided Design*, San Jose, CA, 1995, pp. 20–25.

**Taku Uchino** received the B.S. degree in physics from Kyoto University, Japan, in 1988, and the M.S. and Ph.D. degrees in physics from Tokyo Institute of Technology, Japan, in 1990 and 1993, respectively.

He was with Toshiba Corporation, from April 1993 to December 2001, and with the Computer Science Department of University of California, Los Angeles, as a Visiting Researcher, from August 1999 to February 2001. Currently, he is with Toshiba America Electronic Components. His research interests include interconnect modeling, power estimation, and signal integrity.

**Jason Cong** (F'99) received the B.S. degree in computer science from Peking University, in 1985, and the M.S. and Ph.D. degrees in computer science from the University of Illinois, Urbana-Champaign, in 1987 and 1990, respectively.

Currently, he is a Professor and Co-Director of the VLSI CAD Laboratory in the Computer Science Department of University of California, Los Angeles. His research interests include layout synthesis and logic synthesis for high-performance low-power VLSI circuits, design and optimization of high-speed VLSI interconnects, FPGA synthesis, and reconfigurable architectures. He has published over 150 research papers and led over 30 research projects. He was appointed as a Guest Professor of Peking University in 2000.

Dr. Cong received the Best Graduate Award from Peking University in 1985 and the Ross J. Martin Award for Excellence in Research from the University of Illinois at Urbana-Champaign in 1989. He received the NSF Young Investigator Award in 1993, the Northrop Outstanding Junior Faculty Research Award from UCLA in 1993, the IEEE TRANSACTIONS ON COMPUTER-AIDED DESIGN Best Paper Award in 1995, and the ACM and SIGDA Meritorious Service Award in 1998. He received an SRC Inventor Recognition Award in 2000 and was the recipient of the SRC Technical Excellence Award for Year 2000. He served as the General Chair of the 1993 ACM/SIGDA Physical Design Workshop and as Program Chair and General Chair of the 1997 and 1998 International Symposium on FPGAs, respectively, Program Co-Chair of the 1999 International Symposium on Low-Power Electronics and Designs, and on program committees of many major conferences, including DAC, ICCAD, and ISCAS. He is an Associate Editor of IEEE TRANSACTIONS ON VERY LARGE SCALE INTEGRATION SYSTEMS and *ACM Transactions on Design Automation of Electronic Systems*.